scientific reports

Check for updates

OPEN

Order–disorder phase transitions of phosphorene and their application to adiabatic quantum computing

Iman Gomrokizadeh[1], Farzaneh Shayeganfar[1]✉, S. Mojtaba Tabatabaei[2] & Ali Ramazani[3]

Phosphorene monolayers exhibit a range of advanced functional properties; however, their spin configurations and structural phase transitions remain unexplored in the context of enhancing performance in quantum computation and information. In this study, we employ a two-dimensional (2D) Ising model with nearest- and next-nearest-neighbor interactions, denoted as J and J' respectively, alongside a Monte Carlo approach, to investigate the structural phase transitions and spin behavior of phosphorene. Using this model, we derive the temperature-dependent phase diagram of the phosphorene in terms of the interaction strength ratio (J/J'), revealing three distinct phases—checkerboard-ordered, glassy, and quasi-ordered—with a phase boundary at $J/J' = 2$. Additionally, we analyze the effects of possible defects and strains in the phosphorene lattice induced by the substrate on the phase transitions. Our findings have potential applications in adiabatically switching states through gradual variations in coupling constants, offering new possibilities for adiabatic quantum computing (AQC) and π-ring arrays.

Keywords Phosphorene, 2D Ising model, Monte Carlo, Phase diagram, Glassy state, Domain wall length, Adiabatic quantum computing (AQC), Spin frustration, Order–disorder transition

The discovery of graphene[1] marked a milestone in the field of 2D materials, leading to the theoretical and experimental exploration of numerous other 2D materials with experimentally verified properties[2–8]. Among these, phosphorene stands out due to its unique properties and potential applications[9–12]. Phosphorene, an atomic monolayer of black phosphorus (BP), is more stable than other phosphorus allotropes such as violet, red, and white phosphorus[13,14]. It was first isolated by mechanical exfoliation from bulk BP in 2014[12].

Unlike other widely studied 2D materials, phosphorene exhibits a distinctive puckered-honeycomb structure arising from the sp^3 hybridization of its atomic orbitals. This structural feature underpins its unique properties, including a thickness-dependent direct bandgap (0.3–2 eV), unusual anisotropy, and excellent physical and optical characteristics, which are rarely found in other 2D materials[15–19]. The puckered structure creates two directions, zigzag and armchair, that contribute to the material's anisotropy[10,18,20]. For instance, while graphene has a planar honeycomb lattice[21] and silicene forms a buckled honeycomb structure[22], phosphorene's ridges or "zigzags" are interconnected via covalent bonds at two different heights[23–25]. Peralta, et al.[26] implemented the effective *k.p* Hamiltonian by employing a multiorbital Slater-Koster tight-binding approach to describe spin–orbit coupling (SOC) effect of Rashba in single layer phosphorene. Their findings reveal that the intrinsic SOC splits valence bands by 22.4 meV, affecting the electronic properties of single layer phosphorene.

Phosphorene's anisotropic structure makes it a promising platform for simulating quantum systems with non-ideal Ising interactions, such as arrays of π-rings[27] and applications in adiabatic quantum computation (AQC)[28]. A π-ring, consisting of a superconducting loop with Josephson junctions, generates magnetic dipole moments that interact via dipole forces. By introducing an external current, the interaction strengths (J and J') and their ratio can be tuned, making the system analogous to a 2D Ising model. Similarly, AQC employs the adiabatic evolution of a system's ground state through gradual variations in coupling constants, offering potential for optimization problems and quantum simulations. Details on π-rings and their dipole interactions can be found in Refs [27,28]. and are omitted here for brevity.

Despite its promise, the complex puckered structure of phosphorene has limited studies on its possible configurations and structural transitions[29–31]. In this paper, we use a 2D Ising model with antiferromagnetic nearest and next-nearest neighbor interactions on a hexagonal lattice to analyze phosphorene's spin configurations and structural phase transitions. First, we derive a structural phase diagram for phosphorene by

[1]Department of Physics and Energy Engineering, Amirkabir University of Technology, Tehran, Iran. [2]Department of Physics, Kharazmi University, Tehran 1571914911, Iran. [3]Department of Mechanical Engineering, Massachusetts Institute of Technology, Cambridge, MA 02139, USA. ✉email: fshayeganfar@aut.ac.ir

simplifying its atomic arrangement into Ising spins. This enables us to predict a novel structure for phosphorene that can be tested experimentally. Second, we focus on the stable puckered-honeycomb structure and investigate its magnetic properties, identifying two distinct spin orders and a transition between them at a critical ratio of coupling constants. We also find a glassy state at low temperatures within a certain range of coupling constants.

Model description and methods

Geometric structure

Our study in this paper mainly focused on two major topics. First, a brief structural study of phosphorene, second a comprehensive spin configuration study of the puckered-honeycomb structure of phosphorene. In the former case, the puckered-honeycomb structure of phosphorene is plotted in Fig. 1a, which contains two ridges of P atoms located at two different heights, alternatively. The P atoms in each ridge are connected to each other by covalent bonds, forming a zigzag pattern. The bond length of P atoms in a zigzag is $d_1 = 2.224$ Å and the angle between these bonds is $\theta_1 = 96.34^\circ$. Each zigzag of P-atom is connected to two other zigzags at different heights. The vertical distance between these two zigzags can be calculated by determining the bond length connecting the two ridges and the angle of the bond. Every P atom in a zigzag is connected to a P atom in its adjacent zigzag by a covalent band of length $d_2 = 2.244$ Å, oriented to the zigzag plane by an angle equal to $\theta_2 = 71.7^\circ$[9,20,23,32–36]. It is evident that the vertical distance between two upper and lower ridges is equal to $b = 2.131$ Å. So, by knowing all the distances and angles in the puckered-honeycomb structure of phosphorene, we can determine the nearest neighbors and next-nearest neighbors of each P atom. It is also worth noting that the lattice structure of pristine phosphorene is well known and experimentally established. Its conventional orthorhombic unit cell consists of four phosphorus atoms, with the following in-plane lattice

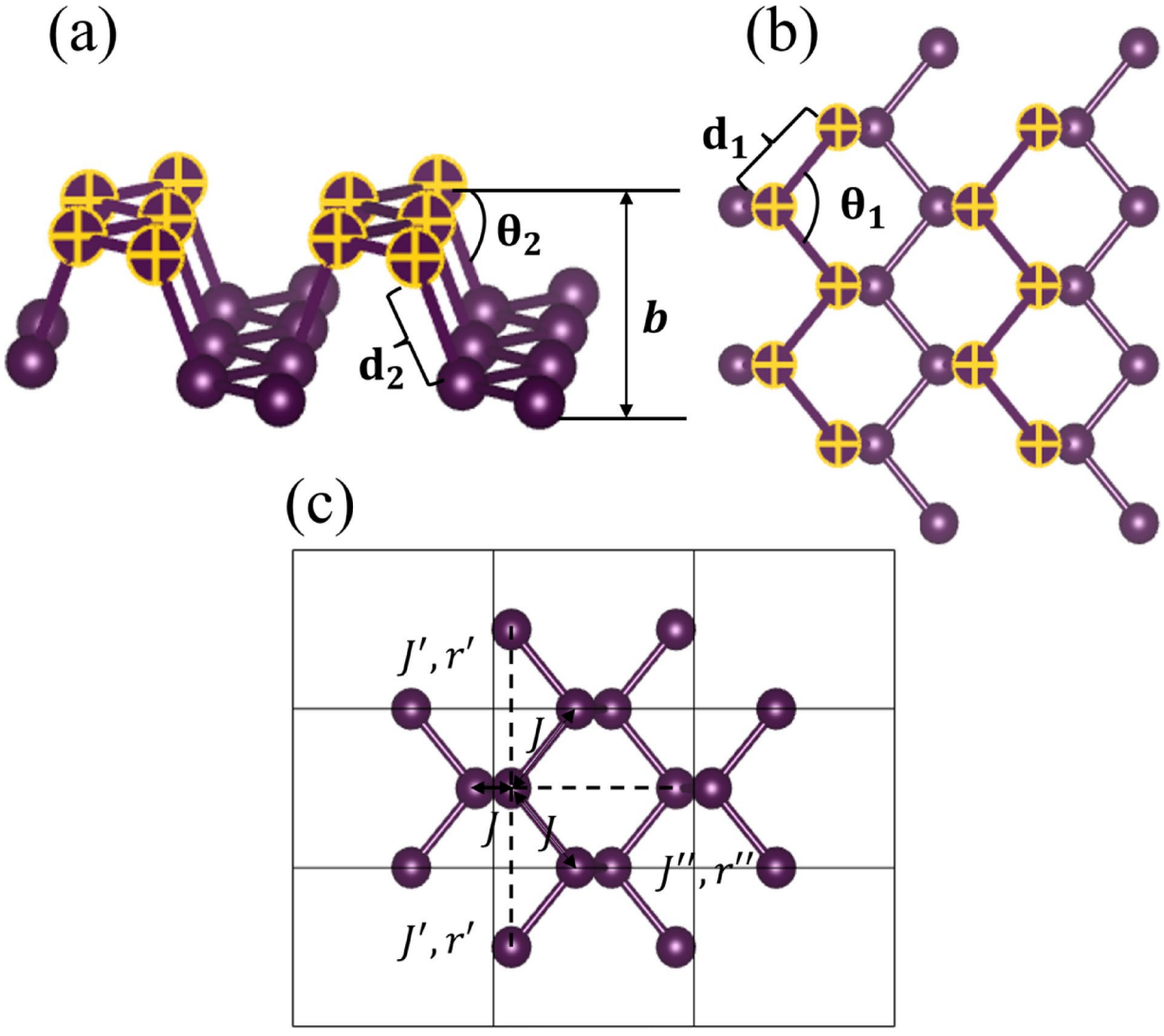

Fig. 1. (**a**) side view, and (**b**) top view of atomic structure of phosphorene (monolayer black phosphorus). There are two upper and lower sublayers (zigzag chains) of P atoms indicated by yellow and purple. (c) Nearest neighbors and next-nearest neighbors denoted by coupling constants J and J'.

constants: $a = 4.58$ Å (armchair direction) and $b = 3.32$ Å (zigzag direction)[16,37]. As shown in Fig. 1, each P atom is connected to two P atoms in the same ridge and to one P atom in an adjacent ridge. These bond lengths differ slightly from each other 0.02 Å. We can ignore this slight difference and consider three nearest neighbors for each P atom. A critical step is to determine the next-nearest neighbors. In the case of graphene, we deal with a flat or slightly buckled honeycomb structure[37], so that for every atom, we have three nearest neighbors and 6 next-nearest neighbors. In the phosphorene case, however, situation is different. Similar to graphene, the top view of phosphorene (Fig. 1b) exhibits a hexagonal pattern, whereas the puckered structure of phosphorene excludes the same length of diagonal neighbors in the hexagonal lattice. In fact, we must calculate every diagonal neighbor in the puckered-honeycomb structure of phosphorene and then determine the next-nearest neighbors of each P atom when studying the spin configurations of phosphorene.

Therefore, by knowing the structure of phosphorene, we can determine whether another possible structure of phosphorene exists. We take every pair of up- and down-atoms next to each other as an Ising spin. Therefore, we estimated the puckered-honeycomb crystal of phosphorene as a flat square lattice and identified two structural phases and their transition points.

Ising model

The main objective of our work was to study the *spin configurations* of phosphorene with a puckered-honeycomb structure and obtain the phase diagram. This is because the puckered-honeycomb structure is the most stable structure of phosphorene observed. While direct studies on spin configurations and order–disorder transitions in phosphorene are scarce, related research in two-dimensional (2D) materials offers valuable insights. For instance, studies on 2D boron–carbon systems have observed order–disorder transitions, which may provide analogies applicable to phosphorene[38]. Similarly, investigations into layered and 2D carbides have demonstrated entropy-driven order-to-disorder transitions, highlighting the significance of entropic effects in 2D materials[39]. Additionally, the classic two-dimensional Ising model with nearest-neighbor interactions has been extensively studied to understand order–disorder phase transitions, offering theoretical frameworks that could be adapted to phosphorene's unique lattice structure[40]. These studies collectively enhance our understanding of phase transitions in 2D systems and may inform future research on phosphorene's spin configurations. To study the spin behavior of the puckered-honeycomb phosphorene, we used a 2D Ising model with nearest and next-nearest neighbors. The reason that we are allowed to use the 2D Ising model to describe the spin behavior of the puckered-honeycomb structure of phosphorene is that we just want the implications for the AQC field, where there are two-state magnetic moments for each π-ring. To properly describe the dipole character of the interaction between the orbital moments, we included the constant of the next-nearest neighbor interaction in the model. In our model, we only considered the first and second neighbors because the spin interactions decrease with the distance between moments as $1/r^3$, so the farer neighbors are slightly affected by the changes of a spin. As Fig. 1c shows, we have two types of diagonal neighbors, J' and J''. Knowing the bond lengths and their angles, we can calculate both the J' and J'' distances. The distance related to J' interaction is equal to $r' = 3.314$ Å and the distance of the J'' interaction is equal to $r'' = 3.622$ Å. We consider the lower distance the next-nearest neighbor. Therefore, in the puckered-honeycomb structure of phosphorene there are three nearest neighbors and two next-nearest neighbors for every P atom. Regarding the $\frac{1}{r^3}$ decrease of orbital moments, the values of J and v are given by $\frac{J}{J'} = \left(\frac{r'}{r}\right)^3 = \left(\frac{3.314}{2.244}\right)^3 = 3.221$, but we consider a more general case where their values are arbitrary.

In order to obtain the phase diagram of P atom spins in phosphorene, we used a 2D Ising model with the next-nearest interactions described by Hamiltonian[41]:

$$\mathrm{H} = \mathrm{J} \sum_{\langle \mathrm{i,j} \rangle_{\mathrm{nn}}} \mathrm{s_i s_j} + \mathrm{J'} \sum_{\langle \mathrm{i,j} \rangle_{\mathrm{dn}}} \mathrm{s_i s_j} \tag{1}$$

where the two-valued Ising spin variable s_i can be $+1$ or -1. There are two competing antiferromagnetic nearest neighbor and next-nearest neighbor interactions, J and $J' > 0$. Here, J and J' denote the strength of interactions between spins. Since in our model, Ising spins represent the actual P atom spins, J and J' describe the strength of interactions between P atom spins. $\langle i, j \rangle_{nn}$ denotes the summation over sites i and j that are nearest neighbors, and $\langle i, j \rangle_{dn}$ denotes the summation over sites i and j that are next-nearest neighbors (two out of six diagonal neighbors).

Here, it is important to emphasize that we are aware of the complexity of the phosphorene lattice, particularly due to its puckered structure arising from sp^3 hybridization. To account for this complexity in the model, we can define two types of nearest neighbors: the first along the same zigzag direction and the second along adjacent zigzags. The phosphorene lattice arising from sp^3 hybridization can be accounted by defining two distinct types of nearest neighbors. Specifically, instead of using interaction strengths J and J′ for nearest and next-nearest neighbors, we can assign J_1 to nearest neighbors along the zigzag direction (same ridge), J_2 to nearest neighbors along the armchair direction (adjacent ridges), and J′ to next-nearest neighbors. Using this approach, we could construct a four-dimensional plot of specific heat peaks as a function of J_1/J', J_2/J', and T/J'. Similarly, the phase diagram would become three-dimensional, plotted as J_1/J' versus J_2/J' versus T/J', instead of the current two-dimensional representation. In this approach, The Hamiltonian introduced in Eq. (1) transforms into the following Hamiltonian:

$$\mathrm{H} = (J_1 + J_2) \sum_{\langle \mathrm{i,j} \rangle_{\mathrm{nn}}} \mathrm{s_i s_j} + \mathrm{J'} \sum_{\langle \mathrm{i,j} \rangle_{\mathrm{dn}}} \mathrm{s_i s_j}. \tag{2}$$

This analysis is included in supplementary information (SI) Sect. 5, where we demonstrate that using simplified model with only one type of nearest neighbor is justified (Fig. S4).

The other possible modification is to include the interaction between spins and the lattice (i.e., spin-phonon interaction) in our model. However, in this study, we have considered a fixed, static lattice geometry, meaning that phonons or structural deformations in phosphorene are absent. Therefore, we can safely neglect the presence of phonons and their interactions with spins in our analysis.

Monte Carlo simulation, phase diagram and defects

We implemented a Monte Carlo simulation to calculate the phase diagram. When working with the partition function and then the specific heat, we usually confront the parameters $\alpha = J/J'$ and $t = T/J'$. In Monte Carlo simulations for every α and t, we can find the transition point at which the configuration of the system changes from an ordered state to a disordered state. These transition points are identified from the peaks at specific heat. There is also a glassy state at low temperatures, which changes from a glassy to an ordered state. We applied two types of Monte Carlo simulations: quenched and annealed Monte Carlo. In order to simulate the Infinite lattice and also eliminate edge effects, the boundary condition used in the simulation is considered to be periodic. Using annealed Monte Carlo, we cannot observe any sign of a glassy state. This is due to the difference between these two methods, which details of both are presented in SI.

While other analytical or numerical techniques, such as exact diagonalization[42] or renormalization group (RG) analysis[43], could in principle provide additional insights, they are not well suited to the complexity of the anisotropic, puckered phosphorene lattice with next-nearest-neighbor interactions. Exact diagonalization is limited to very small system sizes, and RG methods typically rely on translational symmetry and simplified interaction terms. In contrast, Monte Carlo simulations—particularly with the Metropolis algorithm—remain the most suitable and widely adopted approach for studying spin configurations and phase transitions in geometrically complex 2D systems. Given that our focus is on identifying distinct spin phases and constructing a qualitative phase diagram, rather than extracting critical exponents with high precision, the Monte Carlo method provides a reliable and appropriate framework for our study. This is further supported by a low-temperature analytical calculation on a simplified unit cell, presented in Sect. 3 of the Supplementary Information, which confirms the consistency of our phase boundary behavior.

As we discussed, we can find the phase transitions by calculating the specific heat for various J/J' ratios and temperatures. Then we find peaks in specific heat and its corresponding J/J' ratio and temperature. Therefore, for every J/J' ratio, we have a temperature at which different spin orderings exist above and below that. This can be a challenging task, because of topological defects. Defects are natural phenomena that occur in all crystal types[44]. Defects may arise in ordered states as disordered narrow regions or boundary layers. These narrow regions form domains with regular patterns separated by boundaries. We refer to these narrow regions or boundaries separating two ordered states as domain walls. The closer we get to the phase transition border in the phase space, the more defects we observe. Perfect crystal can be obtained Only at large J/J'.

Furthermore, we can analytically study some defects in the phosphorene structure, which lead to a better insight of the actual lattice. A typical defect that could arise in an ordered lattice is just a boundary between two different orderings, checkerboard and checker-stripy. Checker-stripy is a different ordered phase that we will study in the continuation of this paper, that is a hybrid of checkerboard and stripy order. We call this defect a domain boundary. To calculate the energy per site for the flat and corner portions of this domain boundary, we took a six-site plaquette around point A, as shown in Fig. 2a, and calculated the energies of sites numbered from 1 to 6. We can do the same for the dislocation defect, as shown in Fig. 2b, c. (see SI (Sect. 2) for computational details on different types of defects, as shown in Fig. S1a–c).

An important question regarding the different phases in the phosphorene lattice is their degree of stability. In the next section, we assess the stability of the four observed phases—checkerboard, checker-stripy, paramagnetic, and glassy—through a detailed analysis. By tracking key observables such as energy, domain length (DL), and magnetization over Monte Carlo time, along with evaluating the autocorrelation function, we find that the checkerboard phase is fully stable, while the checker-stripy and glassy phases are metastable. In contrast, the paramagnetic phase exhibits instability.

Adiabatic quantum computing

The discussions above were only about the case of suspended phosphorene, where the ratio of interactions is constant and equal to, $J/J' = 3.221$. However, we can control the coupling interaction J and J' and their ratio using an external agent in π-rings system. A π-ring, consisting of a superconducting loop with Josephson junctions, generates magnetic dipole moments that interact via dipole forces. Thus, an array of π-rings that have magnetic moments perpendicular to the plane of the rings can be treated as Ising spins, and interactions via magnetic dipole forces can be shown by antiferromagnetic coupling constants (J and J'). We can also control the strength of the dipole force interactions by adding an additional current between π-rings[45].

Thus, we can create an array of π-rings (Fig. 3) in a hexagonally puckered arrangement. By introducing an additional current passing between π-rings, the coupling interactions can be changed and controlled. We refer to this method as Adiabatic Quantum Computation (AQC)[28]. Figure 3 is sketched to clarify how we use the part of our results related to different spin configurations of phosphorene in the AQC field. The black and white circles represent upward and downward magnetic dipole moments, which refer to spin up and down in analogy with phosphorene atoms. The color of the circles' borders also denotes atoms located at higher and lower heights with respect to each other, in analogy with the puckered form of the phosphorene lattice. One of the major challenges in implementing AQC is the reliance on qubit systems, which require extremely low temperatures and expensive infrastructure. Phosphorene, on the other hand, offers a unique advantage due to its stability at room temperature. This makes it a compelling candidate for use as a testbed for AQC calculations. In the

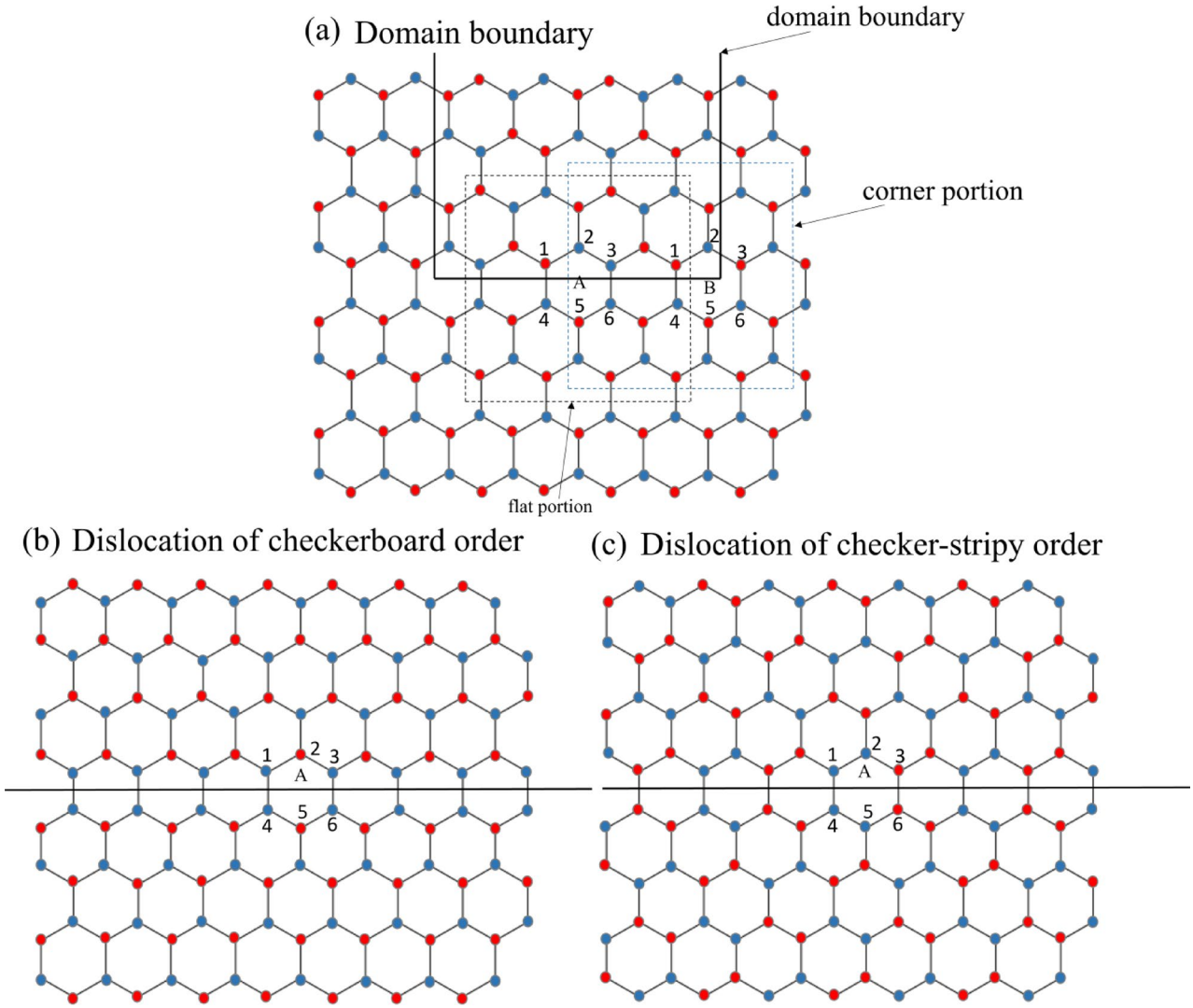

Fig. 2. Two examples of typical defects in a hexagonal phosphorene lattice. Domain boundary between checkerboard and checker-stripy orders (**a**). A dislocation (shift by one lattice constant) in the checkerboard-ordered phase (**b**) and in the checker-stripy-ordered phase (**c**). Blue circles represent "up" spins and red circles denote "down" spins.

Ref[46,47], an example of the systems that is described by the Ising model and can be used as a candidate for AQC calculations is provided. By leveraging the phosphorene lattice, it may be possible to gradually evolve a system from an initial Hamiltonian to a final desired Hamiltonian, following the principles of AQC.

While this idea is in its exploratory phase, we believe that the inherent properties of phosphorene, combined with its compatibility with the anisotropic Ising model, make it a promising platform for AQC research and development.

The AQC and adjustable coupling of multi π-rings systems has been considered experimentally in the ref[48]. The π-ring is usually considered a primary candidate for the flux qubit because of its long decoherence time and low noise[45]. Thus, the planar clusters of π-rings used in AQC are similar to those used with superconducting flux qubits. Therefore, by studying the phosphorene spin configurations, we open a pathway for developing and improving some quantum algorithms. Moreover, by investigating the phase diagram of a puckered-honeycomb π-ring system, one can explore different order and disorder states at different values of J/J' ratios, which can be tuned by controlling the coupling.

Domain wall length

To calculate the phase transition between a glassy state, which occurs at low temperatures, and an ordered phase, we cannot simply use specific heat peaks. In fact, as the temperature decreases, the specific heat value becomes higher because of the $1/T^2$ behavior of the specific heat. Therefore, we must use other criteria to determine the phase transition between the glassy state and other ordered or unordered phases. In order to obtain the border between a glassy state and an ordered state in the phase space, two different order parameters as 'mean domain wall length' (calculated and plotted in Fig. 4) and 'Edwards and Anderson order parameter' are used.

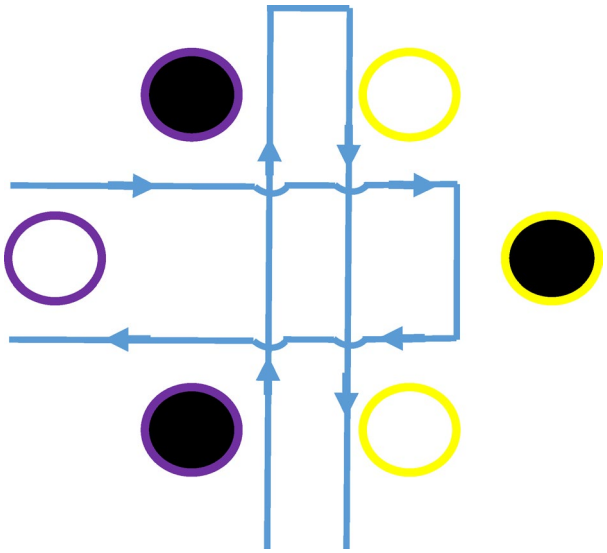

Fig. 3. Adiabatic Quantum Computation (AQC). We can create a set of π-rings that have a magnetic dipole moment upward or downward. We take an analogy of these magnetic dipole moments with spins up and down, shown by black and white. The color of the rings' borders represents atoms in upper and lower planes with respect to each other, in analogy with puckered-honeycomb structure of phosphorene. By adding an additional current, a magnetic field is created between the π-rings. Thus, the coupling strength between the π -rings can be changed and controlled.

We calculated the mean domain wall length order parameter and the change in the specific heat to obtain the phase transition points in the $T/J' - J/J'$ phase space. At very low temperatures, a disordered state exists that differs from a paramagnetic state. We can consider this disordered state as an ordered state containing frozen topological defects. We call these topological defects frozen because there is not enough energy in the system to exit this configuration and form another configuration with new topological defects. In fact, each configuration that the system takes corresponds to a local minimum, which the system remains at. Within these defect boundaries, we see small ordered regions. At very low temperatures, all different configurations (energy minima) are separated by high barriers, so each configuration is locally stable. As we increase the temperature, the height of the energy barriers decreases; thus, the order is restored, including defects throughout the ordered state. In fact, we observe large ordered domains separated by disordered narrow regions that one may call boundary layers or domain walls.

We know so far that the glassy state is a state in which various ordered domains are separated by numerous frozen topological defects. This is related to a phenomenon called the proliferation of defects. Therefore, the key to determining the glassy state is to study domain boundaries or "Domain wall length" (DL) as plotted in Fig. 4 where its calculation is included in SI.

Strain effect

Finally, the effect of strain on transition points in the phase diagram is investigated. For real phosphorene on a substrate, there is always an intermolecular interaction due to the interaction of atoms (spins) with the substrate. Considering this spin–lattice interaction, the transition points in the phase diagram significantly change. The spin–lattice interaction is shown by a spin–lattice coupling term $f \sum_i s_i u_{ij}$[49], so Eq. (1) becomes:

$$\mathrm{H} = \mathrm{J} \sum_{\langle \mathrm{i,j} \rangle_{\mathrm{nn}}} \mathrm{s_i s_j} + \mathrm{J'} \sum_{\langle \mathrm{i,j} \rangle_{\mathrm{dn}}} \mathrm{s_i s_j} + \mathrm{f} \sum_{\mathrm{i}} \mathrm{s_i u_{ij}} \tag{3}$$

where the first sum is taken over all nearest neighbors, and the second sum is taken over all next-nearest or diagonal neighbors. The third term is the spin–lattice coupling term, which consists of the interaction forces of spins and out-of-plane displacements of atoms in the third dimension (vertical direction). u_{ij} is the elastic tensor and is given by[49]:

$$\mathrm{u_{ij}} = \frac{1}{2} \left(\partial_{\mathrm{i}} \mathrm{u_j} + \partial_{\mathrm{j}} \mathrm{u_i} + \partial_{\mathrm{i}} \mathrm{h_a} \partial_{\mathrm{j}} \mathrm{h_a} \right) \tag{4}$$

where h_a is the out-of-plane displacement. Moreover, f in Eq. (3) is expected to decay exponentially as $f = f_0 e^{-r/\xi}$ where ξ is the length scale. Therefore, because of this exponential decay, we ignore next-nearest neighbor interactions and consider only nearest neighbors spin–lattice interactions for the third term in Eq. (3). Therefore, we again performed Monte Carlo simulations for the Hamiltonian in Eq. (3), which includes an

extra term of spin–lattice interaction, for different tensile (positive) and compressive (negative) strains. The results are shown in SI; Fig. S3, where their phase transition maps indicate a boundary shift of stripy, glassy and checkerboard states. There is also an analytical study of the phase diagram behavior at the low-temperature limit (see Sect. 3 of SI) for both suspended phosphorene (without strain), and phosphorene on a substrate (with strain) (Fig. S2). We have also provided spin configuration snapshots of the phosphorene lattice under different strain values in the Supplementary Information (Sect. 7, Fig. S8). These snapshots show complete agreement with the phase diagrams of strained phosphorene, further confirming the accuracy of our phase characterization.

Results and discussion

Phosphorene's structure

Our systematic study begins with the 2D Ising Hamiltonian in Eq. (1) implemented for the phosphorene structure, as explained in the previous section. We replaced every spin with the value $s_i = +1$ with two P atoms next to each other, while the left one is upward and the right one is downward, and vice versa for $s_i = -1$. If we do this, the checkerboard ordering turns into the well-known puckered-honeycomb structure of phosphorene. Performing the same replacement in the stripy phase yields a completely different structure. In stripy ordering, each P atom is connected to one P atom at the same height and to two P atoms at different heights. We do not intend to investigate this new structure and study its nearest and next-nearest neighbors and its magnetic properties. We just note that there is a possibility that a new structure of phosphorene can be prepared in the laboratory by changing the interaction constants J and J'. For different 2D crystals forming a monolayer like phosphorene on different substrates, the $\frac{J}{J'}$ ratio can vary within a rather broad range. Therefore, at least by theory, we can probably make a phosphorene layer with a completely different structure from the usual puckered-honeycomb. However, we cannot determine the lattice constants of this new phosphorene structure using the Ising model, as this lies beyond the capabilities of our approach and the scope of this paper. Nonetheless, the potential existence of such a structure may motivate future theoretical and experimental investigations into its properties (Fig. 4).

Spin configurations and phase diagram

The second and main section of this paper focuses on the different spin configurations of the most common structure of phosphorene. If we take both nearest-neighbor and next-nearest neighbor coupling constants J and J' of the same sign, the frustration will arise in the system. The effects originating from the interplay between frustration and fluctuations in 2D quantum spin systems have been thoroughly studied recently, both theoretically[50–53] and experimentally[54,55]. We performed Monte Carlo simulations of the Ising model, focusing on the phosphorene parameters ($J/J' = 3.2$), and obtained the phase diagram. As shown in Fig. 5, a set of points separates ordered and disordered phases. As we discussed in "Model description and methods" section, the peaks at the specific heat identified the transition points (We further analyzed the total energy and magnetization behavior, along with specific heat peaks and domain wall length variations, to more precisely confirm the locations of the phase transition points. In Sect. 8 of the Supplementary Information, we present plots of energy and magnetization as functions of temperature for various values of J/J' (Fig. S9). These results are in strong agreement with the transition points identified in the phase diagram shown in Fig. 5). There is also a glassy state in which we can determine the borders using the mean wall length order parameter and the change in specific heat. We consider the glassy state when various ordered domains are separated by numerous frozen topological defects. The glassy state occurs at very low temperatures. At very low temperatures, all different configurations (energy minima) are separated by high barriers. We can clearly observe from Fig. 5 that by increasing the temperature, the system enters an ordered state. It is because by increasing the temperature, the height of the energy barriers decreases, so the order is restored. Naturally, defects can be observed in this ordered phase. In fact, what we observe are large ordered domains separated by disordered narrow regions that one may call boundary layers or domain walls. There are two types of orders. At $J/J' > 2$ the order is checkerboard. In this order, each spin is surrounded by three opposite spins. O'Hare et al.[37] reported that at $J/J' < 2$ there is a new type of order not observed in graphene. The type of order observed in phosphorene at $J/J' < 2$ was not a typical specific order, like the checkerboard order. In this order, there are double stripes (up-down and down-up spin pairs) repeating alternately horizontally, but there is no order in the vertical repeat. It is a hybrid of checkerboard order and stripe order, the *checker-stripy* order. Unidirectional charge density wave states (CDW) or stripe order has been observed in several quasi 2D strongly correlated materials over a range of temperatures[56,57]. The stripe order characterization has been considered as a potential order phase in high temperature superconductivity among several quenched disorders[58,59]. As stated previously, this is a quite new order and may provide new electronic and magnetic features for systems with this type of ordering. There are several experimental evidences of stripy spin configuration such as Gao et al.[60] and Gye et al.[61], where they show that strain or accidental doping create a triangular stripe transition at the surface. Moreover, Zhu et al.[62] reported Mott localization in Iron oxychalcogenides, where they figured out its magnetic properties by implementing a doubled checkerboard spin building blocks. Moreover, the formation of checkerboard and stripe patterns; hybrid and the transition between these two patterns has been observed in a stack of driven quasi-1D homogeneous dipolar condensates[63], where the emergence of transient checkerboard and stripe patterns can also extend two-dimensional multi-layer dipolar Bose- Einstein condensates.

In many strongly correlated materials, inhomogeneous orders compete as a common feature[64]. For instance in the high-temperature cuprate superconductors; inhomogeneous orders of spin, charge and pair density waves emerge as unidirectional stripes to checkerboards[65,66]. Experimental evidences reveal that this observed inhomogeneous orders compete with pseudogap physics and distinct from that[67,68]. To investigate the inhomogeneous order of superconductors, Zheng et al.[69] studied the stripe order in the underdoped region of correlated electron systems by using the two-dimensional Hubbard model.

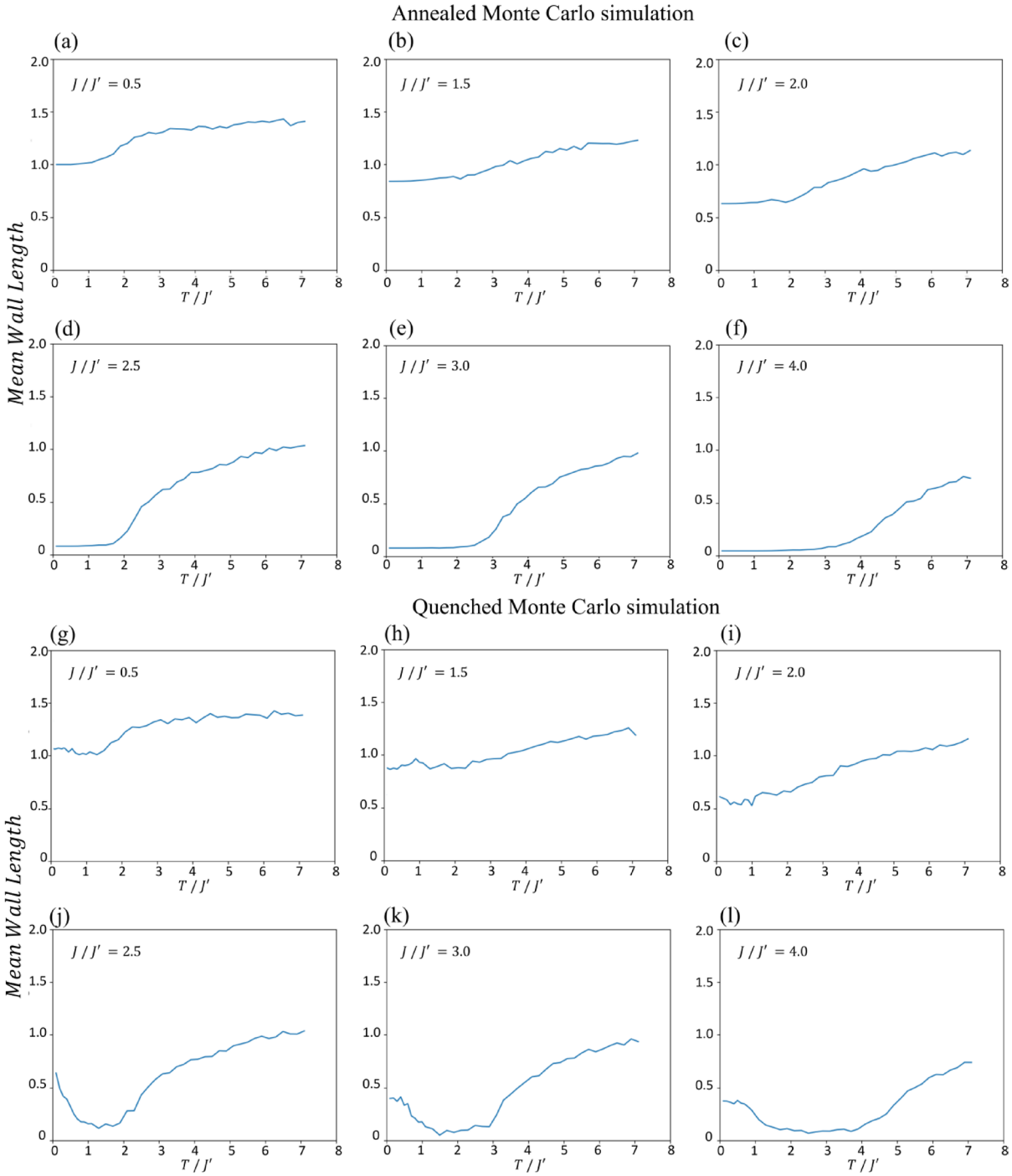

To realize a spin liquid state, the standard approach is based on magnetically frustrated states, which rely on spin configuration and interaction. Dronova et al.[70] proved the existence of long-range spin interaction on pyrochlore lattice, creating a 3D checkerboard spins structure as a long-range order.

In the case of phosphorene, with three nearest neighbors and two next-nearest neighbors, only checkerboard order is observed. This is because the $\frac{J}{J'}$ ratio for phosphorene is $\frac{J}{J'} = \left(\frac{r'}{r}\right)^3 = \left(\frac{3.314}{2.244}\right)^3 = 3.221$. Thus, the order is in the checkerboard region. Of course, by growing phosphorene on different substrates, we can change the $\frac{J}{J'}$ ratio and obtain the checker-stripy order. Therefore, considering the potential existence of this new phase under the specified conditions and its placement in the phase diagram, we hope this finding will encourage future experimental or first-principles investigations. If we further increase the temperature, the direction of spins becomes random. In this paramagnetic state, no order can be observed, and no specific domain wall or notable regular pattern. Figure 8 shows snapshots of suspended phosphorene and phosphorene on a substrate. You can clearly see the checkerboard order in the case of suspended phosphorene and the checker-stripy order in the case of phosphorene on a substrate. The paramagnetic state at higher temperatures is also shown. We also show the phase diagrams in three dimensions in Fig. 6. The transition phase line is observable by the light blue.

◀**Fig. 4**. Mean length of domain boundaries (mean Domain wall Length (DL)) as a function of temperature for the 2D Ising model with nearest next-nearest neighbor interactions at different values of the parameter $\alpha = J/J'$, where J and J' are the interaction strengths of nearest neighbors and next-nearest neighbors. The DL parameter is described by Eq. (s22). The results of figures (**a**) to (**f**) are obtained from a Monte Carlo simulation with the annealing procedure. For $\alpha < 2$, the mean wall length tends to DL = 1 at low temperatures and for $\alpha > 2$ it tends to DL = 0. It is because of different orders at these two regions (checker-stripy for $\alpha < 2$, and checkerboard for $\alpha > 2$). In the annealed system, there is no evidence of a glasslike state, except for $\alpha = 2$, where the crossover between different types of ordered ground states occurs. It is because that as we lower the temperature, the system restores an ordered state, in which it remains. This behavior arises from the fundamental difference between annealed and quenched Monte Carlo processes. In annealed Monte Carlo, as the temperature is gradually lowered, each simulation begins with the final spin configuration obtained at the previous (higher) temperature. As a result, once the system reaches a temperature where the previous state is already ordered, it effectively starts with an ordered configuration. At these low temperatures, the system lacks sufficient thermal energy to escape from this state, making it unlikely to explore other configurations. In $\alpha = 2$, where the crossover between ordered phases occurs, DL is between 0 and 1 at low temperatures. The results of figures (g) to (l) are obtained from a Monte Carlo simulation without the annealing procedure (quenched system). The steep deviation from 0 at $\alpha > 2$ is a signature of the onset of the glasslike state. It is because that at low temperatures, the system is in a configuration with a high energy barrier and there is not enough energy to escape this situation and restore the order. simulations are done on a 32×32 lattice.

We can also analytically study the behavior of phase diagram, at least at low temperatures. For this purpose, we must consider a unit cell for the phosphorene lattice and then write a partition function for it by knowing the set of energy levels and their degeneracy. We conducted this analytical study for both suspended phosphorene and phosphorene supported on a substrate under various strain conditions, as presented in SI, Fig. S2. Additionally, a Monte Carlo simulation was performed to obtain the phase diagram of phosphorene on a substrate.

Glassy state

There is also a glassy state at very low temperatures. To determine the border between the glassy and ordered states, we cannot simply use peaks associated with specific heat. This is due to the $1/T^2$ behavior of the specific heat. At low temperatures, the specific heat diverges, and it is difficult to determine the exact phase transition between the glassy and ordered states. As we discussed, the glassy state consisted of many small ordered regions separated by boundary layers or domain walls. This behavior is associated with the phenomenon known as defect proliferation. Therefore, to understand the glassy state behavior and determine the exact temperature at which the transition between the ordered state and the glassy state occurs, we calculated the mean DL for each $\frac{J}{J'}$ and each temperature, using two Monte Carlo simulation techniques, namely the annealed Monte Carlo and the quenched Monte Carlo method. As can be seen in Fig. 4, in the quenched Monte Carlo simulation, unlike the annealed simulation, there is a steep deviation at low temperatures. This is a signature of the onset of the glasslike state at low temperatures. In the annealed Monte Carlo, as we lower the temperature, we always start our simulation in an ordered state in which the system remains. This is because the system does not have enough energy to escape from the minimum energy configuration. We see that at $\mathrm{J/J'} < 2$, DL converges to 1, as one can check directly for a checker-stripy order, while at $\mathrm{J/J'} > 2$, DL converges to 0, as we can expect for a checkerboard order. It is worth noting that the value attributed to the checker-stripy order corresponds to an ideal, perfectly ordered configuration—one that does not occur in practice due to the presence of frustration and defects. As a result, the checker-stripy phase cannot remain in a fully stable, long-lived configuration; instead, it gradually shifts between near-degenerate arrangements over time. This dynamic behavior is why we classify it as a *quasi-ordered* phase. One other important result that can be obtained from Fig. 4 is that there is not much difference in the low-temperature behavior for quenched and annealed Monte-Carlo simulation at $J/J' < 2$. This means that there is no glassy state at $J/J' < 2$.

The glassy state warrants further investigation due to its complex and intriguing properties. It is characterized by metastability, slow dynamics, history dependence, and frustration. Based on these defining features, several approaches can be employed to study the glassy state, including analyzing the spin autocorrelation function, tracking the total energy of the system, or evaluating the overlap parameter.

We established the existence of a glassy state at low temperatures for $J/J' > 2$ by examining DL. To further confirm these findings, we now turn to the overlap parameter as an additional diagnostic tool. The method involves considering two independent lattice systems with different initial conditions and evolving them separately. After reaching equilibrium, we compute the overlap parameter q, defined as:

$$q = \frac{1}{N} \Sigma s_i^1 s_i^2 \tag{5}$$

where s_i^1 and s_i^2 represent the spin at site i for the first and second systems, respectively. If the equilibrium state is disordered (paramagnetic), we expect $q = 0$. In the case of a ferromagnetic order, $q = 1$. For a glassy state, q falls within the range $0 < q < 1$, reflecting the presence of multiple local energy minima characteristic of glassy behavior. Furthermore, if this calculation is repeated multiple times and the results are plotted as a histogram, a broad distribution of q is expected, indicating the inherent disorder and frustration in the glassy phase.

We performed these calculations for two values of J/J', 0.5 and 3.5, at both a low temperature ($T = 0.5$) and a high temperature ($T = 2$). We know from the phase diagram (Fig. 5) that the glassy state arises at low

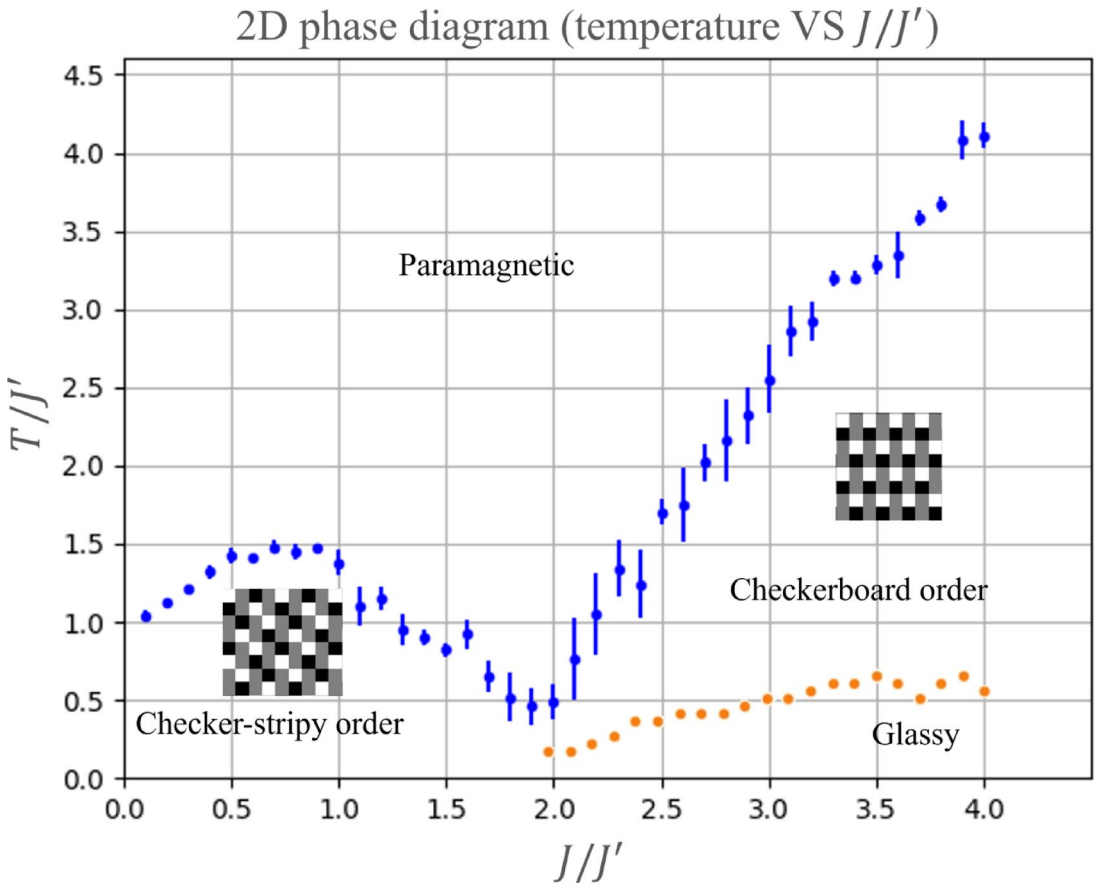

Fig. 5. Phase diagram of phosphorene, calculated by a Monte Carlo simulation for the 2D Ising model with nearest and next-nearest neighbor interactions on a 32×32 lattice, averaged over 20 phase diagrams. The high-temperature phase transition is calculated from the peaks in the specific heat. To improve accuracy, we also tracked secondary observables such as magnetization and domain length to better distinct the phases. The error bars on the phase boundaries represent statistical uncertainty derived from Monte Carlo sampling, as well as thermal fluctuations near critical temperatures. There is another low-temperature phase transition that only obtained from using quenched Monte Carlo simulation and is not observed in the Monte Carlo with annealing, as explained in the Fig. 4. The exact boundary in the low-temperature glassy state phase transition is obtained from change in the magnetization and also an analysis on the spin overlap parameter, described by Eq. (5). There are two orders observed at different values parameter $\alpha = J/J'$. At $\alpha < 2$, there is a new ordered state that opposite double stripes repeat alternately in the horizontal direction, which called it as checker-stripy order. At $\alpha > 2$, the order is the usual antiferromagnetic order, so called checkerboard order, in which each spin is surrounded by spins in opposite directions. Both orders were obtained well away from the transition points, where thermal noise is minimal. Error bars were also calculated to account for the uncertainty arising from thermal fluctuations when approaching a phase transition point.

temperatures of $J/J' > 2$. As anticipated, Fig. 7 clearly shows a broad distribution of q at $J/J' = 3.5$ and low temperature, whereas this broad distribution disappears for $J/J' < 2$. These results provide strong evidence for the presence of a glassy state at low temperatures when $J/J' > 2$.

Figure 8 shows some snapshots at different temperatures for $J/J' = 3.221$ and $J/J' = 1.5$. We can see the checkerboard-ordered state for the puckered-honeycomb structure in the case of suspended phosphorene and the checker-stripy-ordered state for an imaginary phosphorene on a substrate in such a way that J/J' becomes less than 2. To gain better insight into the nature of phase transitions at various J/J' ratios, to observe the formation of different spin configurational phases, and to examine the emergence and annihilation of various types of defects, we provide a series of snapshots for two J/J' ratios—1.5 and 3.2—across different temperatures in Sect. 6 of the Supplementary Information.

Stability assessment

A comprehensive assessment of the thermal stability of the four main spin phases identified in our model—checkerboard, checker-stripy, paramagnetic, and glassy—was carried out using several diagnostics standard in statistical physics. This analysis aims to determine the robustness of the observed phases with respect to thermal fluctuations, Monte Carlo evolution, and initial conditions.

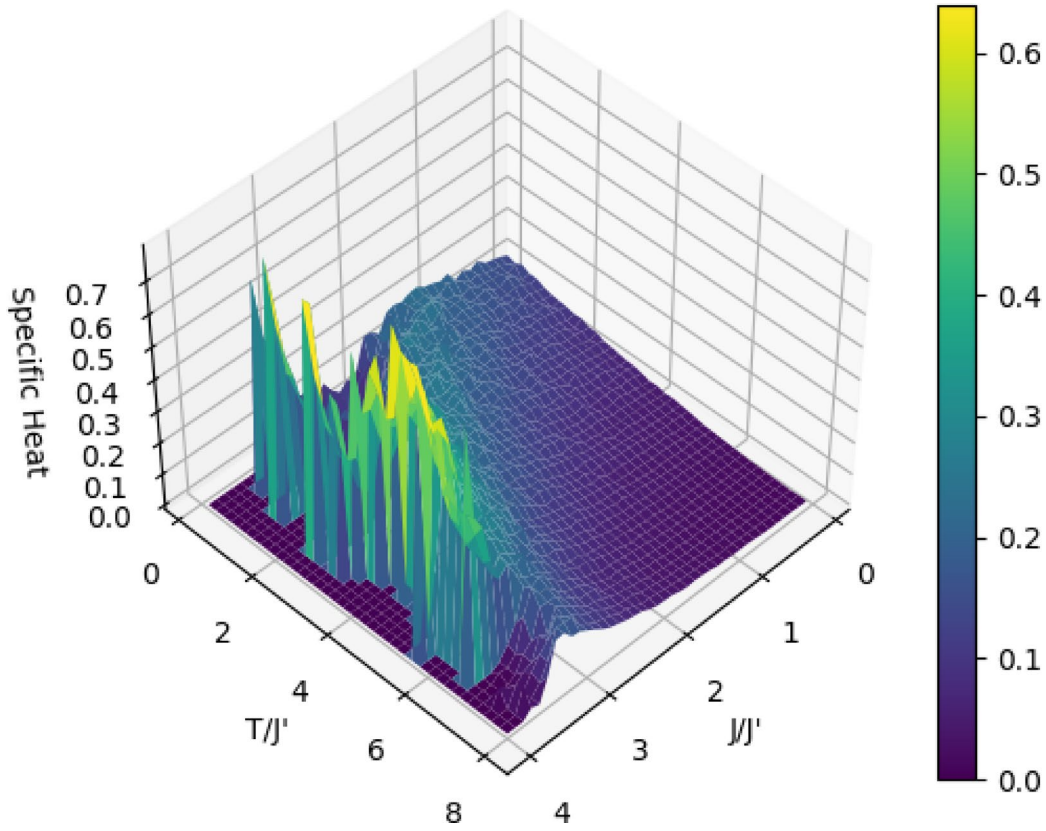

Fig. 6. Three-dimensional phase diagram of phosphorene, on a 32×32 lattice. Rendered using Matplotlib v3.10.1 (Python Software Foundation, https://matplotlib.org/). The peaks shown in Fig. 5 is observable by light blue. We also see an explosion at low temperatures and high J/J', that is sign of a glassy state. Care must be taken to avoid confusing the peaks associated with the glassy state at low temperatures with those indicating phase transitions at intermediate temperatures.

We first evaluated the time stability of key observables over long Monte Carlo simulations at representative points in the phase diagram. Specifically, we tracked total energy, magnetization, and domain wall length (DL). Each of these quantities was measured as a function of Monte Carlo time for fixed values of J/J' and T/J', chosen to represent typical configurations in each phase.

In the *checkerboard phase*, all observables remained stable over time, as shown in Fig. 9a, indicating that the system settles into a robust, energetically favorable configuration and resists thermal disruption. The *paramagnetic phase* (Fig. 9b) exhibited strong and rapid fluctuations in all observables, fluctuating around zero, as expected for a thermally disordered phase. These high-frequency fluctuations around zero indicate that the system is in a completely disordered state, with no long-range temporal coherence, which is characteristic of a paramagnetic unstable phase. The *checker-stripy phase* displayed a distinct behavior, as shown in Fig. 9c: observables fluctuate, but not chaotically. Instead, they oscillate slowly around well-defined values, suggesting some form of persistent but non-unique order. For instance, the domain wall length changes with time, indicating that there is no long-range global order, but the system remains within a class of similar, energetically favorable configurations. This forms the basis of our classification of this phase as quasi-ordered. The *glassy state* (Fig. 9d) on the other hand, is trapped in a local minimum and cannot evolve through the Monte Carlo steps due to insufficient energy at low temperatures. Further explanations of the glassy state will be provided later in the discussion.

To test the reproducibility and uniqueness of each phase, we ran multiple independent simulations, each starting from a randomly initialized spin configuration. In Fig. 4, which plots DL versus temperature for various J/J', each plot is the result of averaging over different simulations. The convergence to the same final state confirms the system's ability to reach its characteristic phase regardless of initialization. Similarly, Fig. 5, the main phase diagram, is constructed by averaging over 20 independent runs. The small error bars across transition lines further support the robustness of the phase identification.

We also computed the autocorrelation function of spin configurations to assess temporal persistence:

$$C(t) = \frac{1}{N} \sum_i s_i(0) \cdot s_i(t) \tag{6}$$

A slow decay of $C(t)$ indicates that the system remains close to its initial configuration for a long time. In addition to the standard linear-scale plot of the autocorrelation function $C(t)$, we also provide a log scale plot

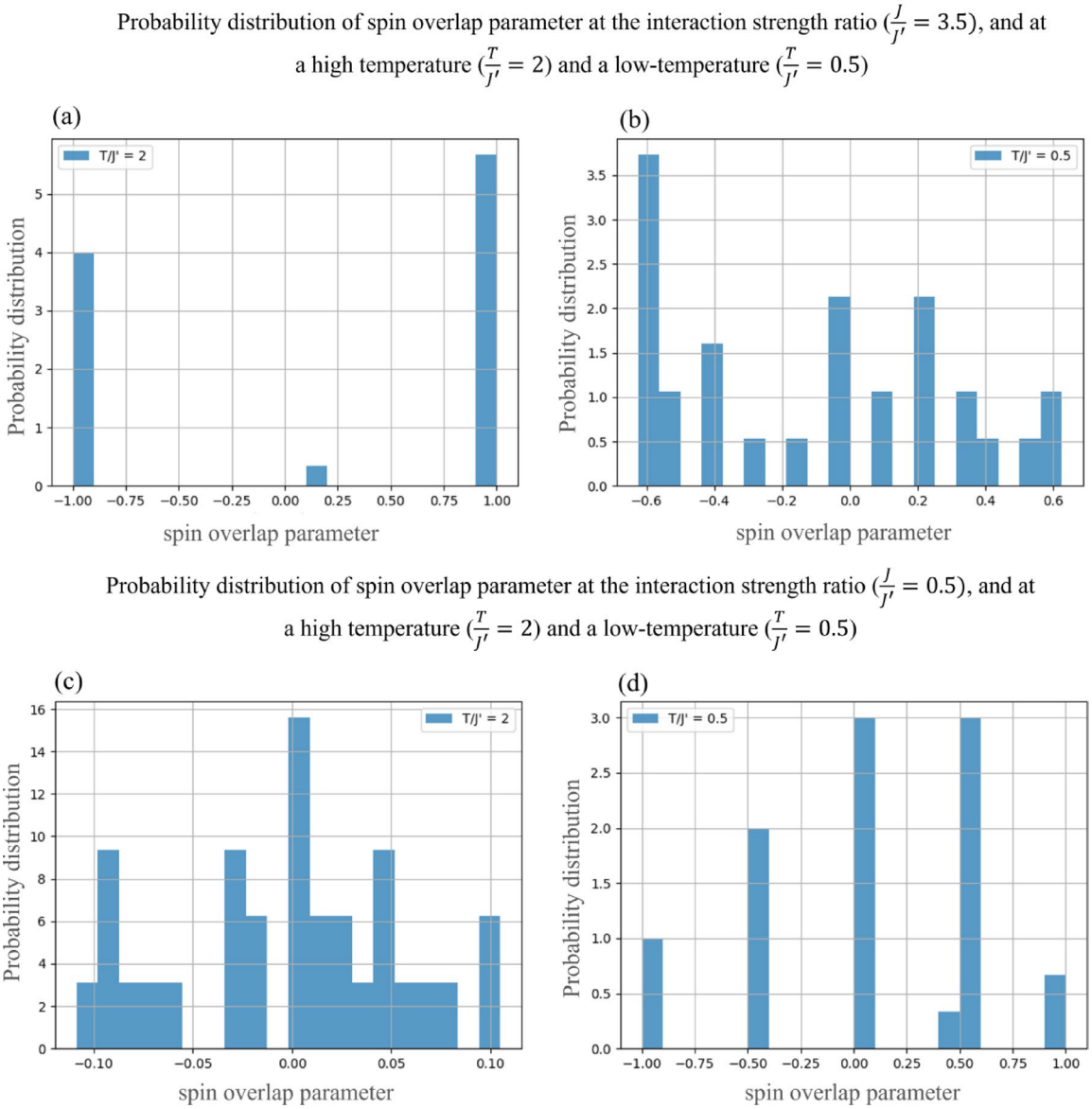

Fig. 7. The probability distribution of the spin overlaps parameter, described by Eq. (5). The spin overlap parameter is calculated 30 times, each for two independent 16×16 lattice, as explained in the results section. We do this at an interaction strength ratio of $\frac{J}{J'} = 3.5$, as a representative of the ratio greater than 2, and at an interaction strength ratio of $\frac{J}{J'} = 0.5$, as a representative of the ratio less than 2. From the phase diagram (Fig. 5), we expect the glassy state behavior at low temperatures of $\frac{J}{J'} > 2$. As it is shown, at high temperature of $\frac{J}{J'} = 3.5$ (**a**), we see two peaks at the values 1 and -1, indicating the checkerboard order. However, at low temperature (**b**), we see a broad distribution of the overlap parameter, which is a sign of glassy state. At the high temperature corresponding to (**c**), we observe a distribution with a peak at zero, which is the expected behavior of a completely disordered (paramagnetic) state. Another important point to note is that, in panel (**d**), one might not initially expect a broad distribution, as the system is in an ordered phase—the checker-stripy phase—rather than a glassy state. However, the checker-stripy phase is a quasi-ordered phase characterized by near-degenerate configurations. In each simulation run, the system can settle into one of these energetically similar configurations, leading to a spread in the measured values. This explains the observed broadness in the distribution. Nevertheless, the spread is not as extensive as in the glassy phase; instead, it clusters around a few specific values corresponding to different checker-stripy arrangements.

for a more detailed tracking of the temporal evolution. The log scale allows us to capture slow changes in the autocorrelation function that might be less noticeable in the linear representation, especially in systems with long decay times or small fluctuations.

As shown in Fig. 10a-b, the *checkerboard phase* showed minimal decay in $C(t)$, remaining close to 1 across long time intervals, consistent with strong long-term stability. The *paramagnetic phase* (Fig. 10c-d), by contrast, shows rapid and high-frequency fluctuations around zero, reflecting its fully disordered unstable nature. The

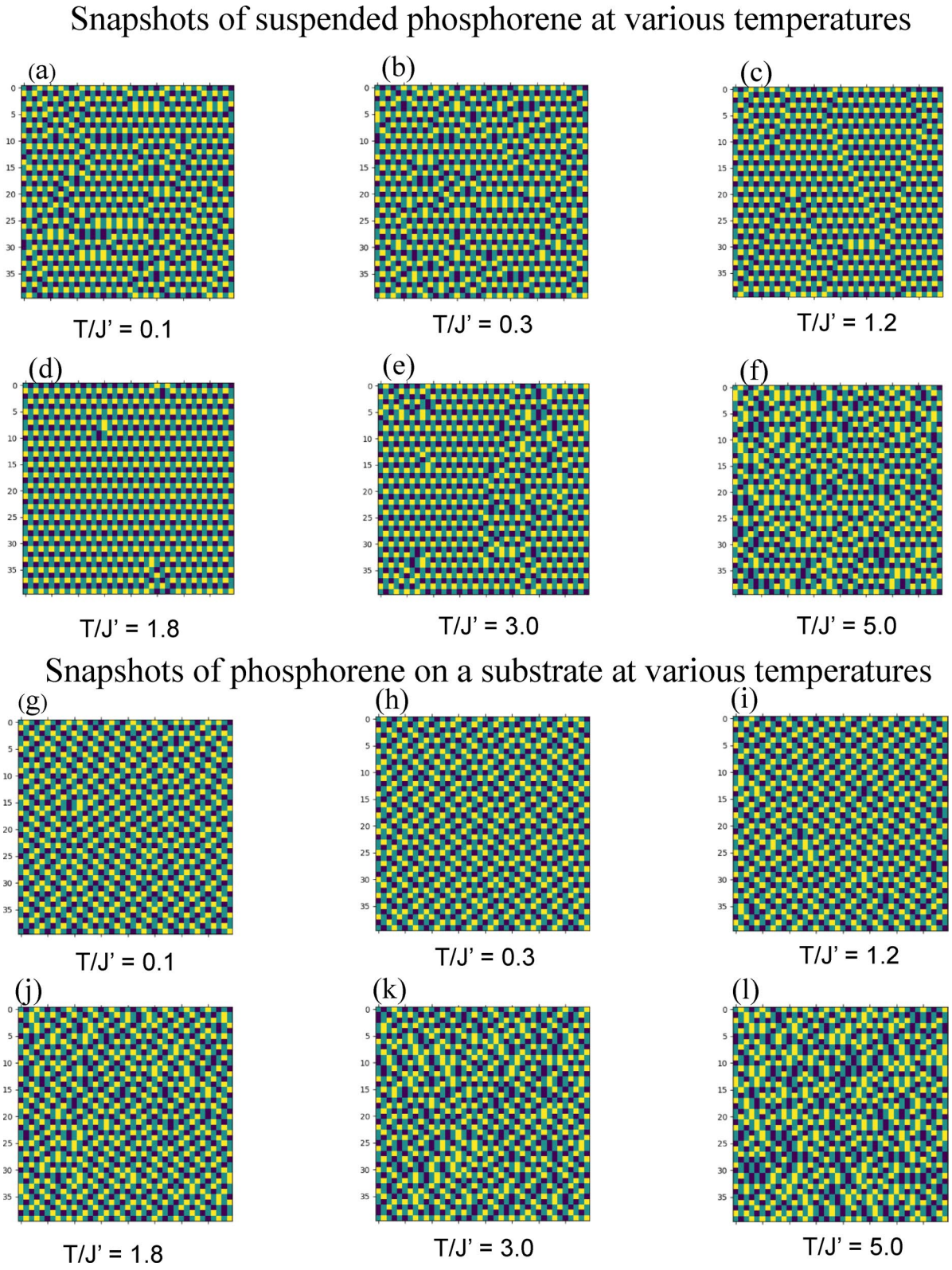

checker-stripy phase (Fig. 10a-b) exhibited slowly decaying oscillations in $C(t)$, with large amplitudes and long wavelengths. This behavior suggests the system is continuously transitioning among a set of near-degenerate states with local order but no globally fixed pattern—further confirming its quasi-ordered nature, and it also shows the *metastability* of this phase. By examining the log-scale plot of $C(t)$, specially for the checker-stripy phase (Fig. 10b), we gain a clearer understanding of its slow decay over time. The gradual decrease and oscillations indicate that the system is not converging to a unique, long-range ordered state. Instead, the system transitions between multiple degenerate configurations, reinforcing our interpretation of this phase as quasi-ordered. This

◀**Fig. 8**. Snapshots of spin configurations at different temperatures for a suspended phosphorene lattice (no strain) with $J/J' = 3^{\frac{5}{2}} = 3.22$ (**a** to **f**) and for a phosphorene on a substrate (strained phosphorene) with $J/J' = 1.5$ (**g** to **l**), where a dark blue square denotes a spin up atom and a yellow square denotes a spin down atom. At very low temperatures for the suspended phosphorene (**a** and **b**) there are small ordered regions separated by frozen defects. This is a glassy state. There are no such small ordered regions separating by frozen defects in the low-temperature configurations of strained phosphorene (**g** and **h**). It means that there is no glassy state at $J/J' = 1.5$. At intermediate temperatures (**c**, **d**, **i** and **j**) the spin configuration becomes partially ordered. This ordered state disappears at high temperatures. At high temperatures (**e**, **f**, **k** and **l**) the spin directions become random. There are no clear ordered regions separating by domain boundaries. This disordered state consists of many short-range defects whose creation is due to thermal fluctuations. To further visualize, understand, and track the spin behavior of the phosphorene lattice—particularly near the phase transition points—we have added to the supplementary information a continuous series of spin configuration snapshots for temperatures ranging from 0.1 to 4.9, in steps of 0.2. These snapshots are provided for two different coupling ratios, $J/J' = 1.5$ and $J/J' = 3.2$, each representing a regime on either side of the transition point at $J/J' = 2$, as shown in Figures S5 and S6. This set of visualizations offers valuable insight into the behavior of different spin phases in the phosphorene lattice, as well as the formation and annihilation of defects across the temperature range. We also highlighted the defects in one of the snapshots of the phosphorene lattice, as shown in Figure S7.

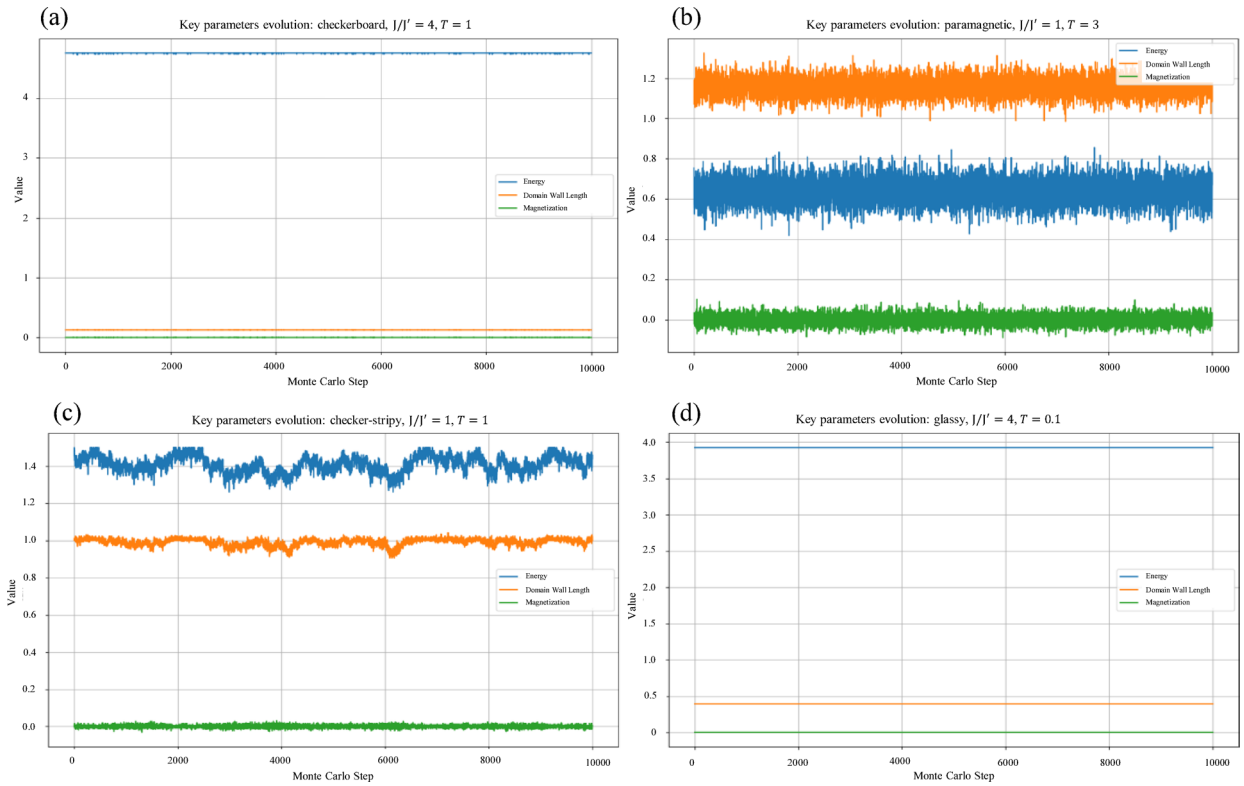

Fig. 9. Evolution of key observables for four typical phases. This figure shows the time evolution of three parameters—energy, domain wall length (DL), and magnetization—for four distinct spin phases: (**a**) Checkerboard, (**b**) Paramagnetic, (**c**) Checker-Stripy, and (**d**) Glassy. In the checkerboard phase (**a**), all observables exhibit slow, minimal changes over time, with occasional small fluctuations, reflecting the system's near-stability and long-range order. The paramagnetic phase (**b**) shows rapid and high-frequency fluctuations around zero for all parameters, characteristic of a completely disordered state. The checker-stripy phase (**c**) displays persistent fluctuations around well-defined values, suggesting quasi-order, where the system transitions between near-degenerate configurations. In the glassy phase (**d**), all observables remain completely constant, with no change in the spin configuration across Monte Carlo steps, indicating the system is stuck in a local minimum due to insufficient thermal energy at low temperatures.

behavior highlights that while the phase retains some form of local regularity, it lacks the global, static ordering found in more traditional, fully ordered phases.

The glassy phase presents unique challenges. At the low temperatures where it occurs, thermal energy is insufficient to overcome the energy barriers separating distinct microstates. As a result, the system becomes dynamically frozen, with spin configurations appearing stable over time.

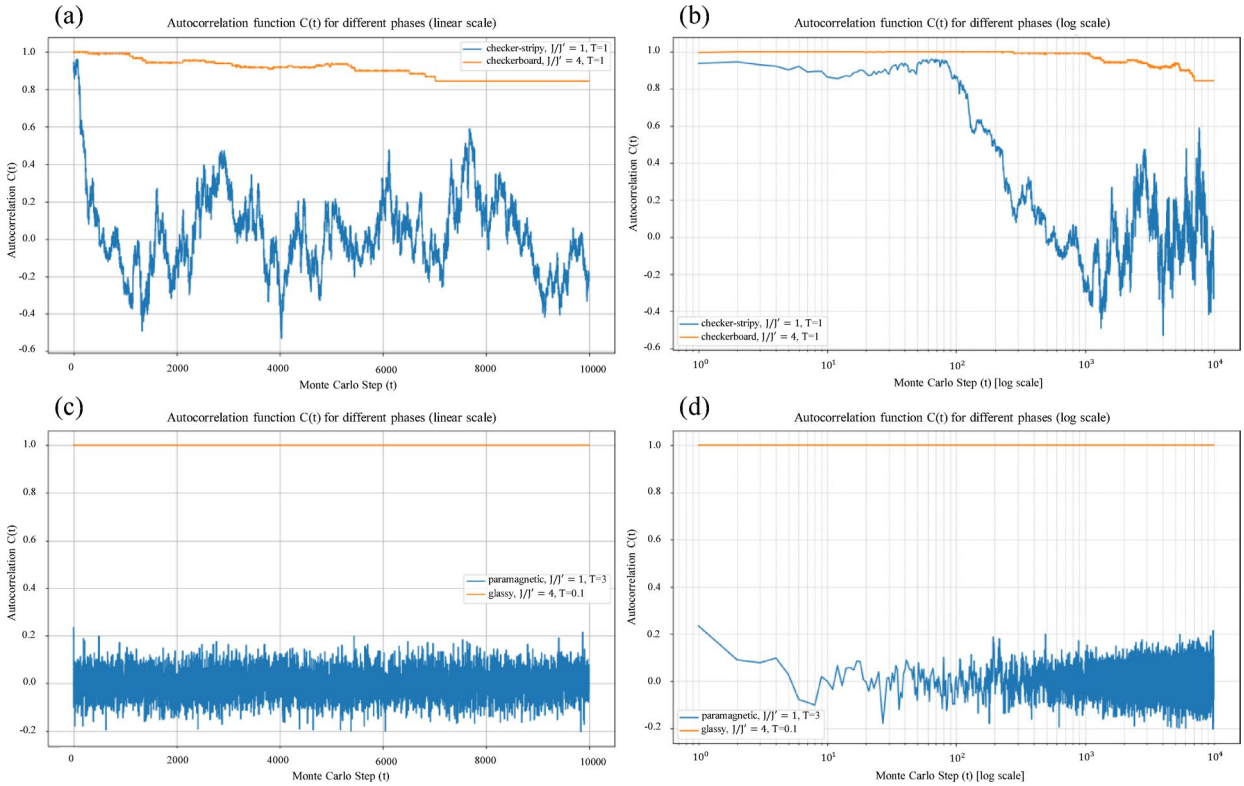

Fig. 10. Autocorrelation function C(t) for different phases over Monte Carlo time. This figure presents the evolution of the spin autocorrelation function C(t) for four phases: (**a**) Checkerboard and Checker-Stripy phases (linear scale), (**b**) Checkerboard and Checker-Stripy phases (log scale), (**c**) Glassy and Paramagnetic phases (linear scale), and (**d**) Glassy and Paramagnetic phases (log scale). In the checkerboard phase (**a**), the autocorrelation function remains near 1, indicating a stable, ordered state with minimal fluctuations over Monte Carlo time. Similarly, the checker-stripy phase (**a**) shows fluctuations, but with a slow decay around well-defined values, suggesting partial stability, though the system transitions between several configurations. The log scale plot of the checkerboard and checker-stripy phases (**b**) reveals the slow decay in C(t) for the checker-stripy phase, where the system fluctuates between distinct values over time, reflecting the multiple stable configurations of this phase. The log scale makes it clearer that the checker-stripy phase gradually shifts between stable configurations but does not settle into a unique, globally stable state, reinforcing its quasi-ordered nature. In the glassy phase (**c**), the autocorrelation function remains constant over time, indicating that the system is trapped in a local minimum, consistent with the lack of available energy to escape this configuration at low temperatures. The paramagnetic phase (**c**) shows rapid fluctuations around zero, confirming its disordered nature.

However, this observed "stability" can be misleading due to ergodicity breaking. We explained before that there are various ways to investigate further the glassy state. One of the best ways is to provide a distribution of spin overlap parameter. So, to investigate further, we performed multiple simulations from different initial spin states. Then calculated the spin overlap parameter q between final states from different runs. Then by analyzing the distribution of q values we can check whether a phase is glassy or not.

In Fig. 7b, the overlap histogram is broad and multi-peaked, indicating that the system settles into many distinct metastable states. This confirms that the glassy phase is not characterized by a single energy minimum but instead by a complex landscape of many nearly-degenerate configurations—a hallmark of spin glass behavior.

These combined results provide a rigorous validation of the thermal stability and dynamical behavior of all identified phases. Our findings align with widely accepted techniques and criteria for assessing stability in Monte Carlo simulations of spin systems[71–73].

Finite-size scaling

To verify whether the critical behavior observed in our simulations holds in the thermodynamic limit, we performed a finite-size scaling (FSS) analysis. In statistical mechanics, it is well known that in an infinite system undergoing a second-order phase transition, thermodynamic quantities such as specific heat C and magnetic susceptibility χ exhibit divergences near the critical point. For finite systems, these quantities remain finite but exhibit scaling behavior with respect to the system size L as follows:

$$C_{max} \sim L^{\alpha/\nu} \tag{7}$$

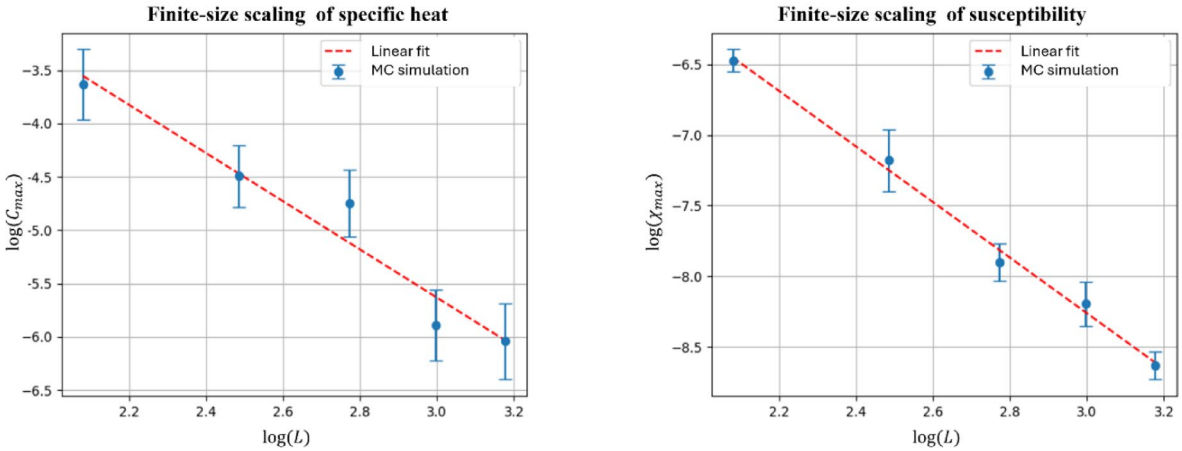

Fig. 11. Finite-size scaling (FSS) analysis of the phosphorene lattice. Each point in the plots represents the peak value of the corresponding observable (specific heat or susceptibility) for a given lattice size. According to finite-size scaling theory, as the lattice size increases, both the specific heat C and the magnetic susceptibility χ are expected to diverge following power laws determined by the ratios of universal critical exponents. As shown in the figure, the data exhibit clear linear behavior on a log–log scale, indicating good agreement with the expected scaling relations. This result supports the validity of our findings and confirms that the critical behavior observed in our simulations extends to the thermodynamic limit of an infinite phosphorene lattice.

$$\chi_{max} \sim L^{\gamma/\nu} \tag{8}$$

here α, γ, and ν are the standard critical exponents, and their ratios help identify the universality class to which the system belongs. To investigate this, we carried out Monte Carlo simulations of the phosphorene lattice using the Ising Hamiltonian described by Eq. (1). We considered square lattices of size L = 8, 12, 16, 20, 24, with interaction parameters $J = J' = -1$. After ensuring equilibration, we computed the peak values of the specific heat C_{max} and susceptibility χ_{max} for each system size.

The results are shown in Fig. 11, where both C_{max} and χ_{max} are plotted against L on a log–log scale. As expected, the data exhibit linear behavior, confirming power-law scaling consistent with finite-size scaling theory. The slopes of these lines yield estimates for the ratios α/ν and γ/ν, respectively. This analysis confirms that the critical behavior identified in our simulations is not an artifact of finite size, and supports the validity of our results for the infinite phosphorene lattice.

Conclusion

In summary, we implemented a 2D Ising model to study the spin configurations of the puckered-honeycomb structure of phosphorene and the transitions between them. To determine the transitions of the ordered and disordered states of phosphorene, we specify the specific heat peak for every J/J', where at $J/J' > 2$ the peaks (the points in the phase diagram) increase by increasing J/J'. In addition, two different spin orderings were revealed depending on the value of J/J'. At $J/J' > 2$, there is a typical checkerboard spin configuration, whereas we observed a new quasi-ordered phase at $J/J' < 2$. We showed that the checker-stripy phase does not have a unique configuration, varying between simulations—hence its classification as quasi-ordered.

There is also a glassy state in the phase diagram. At very low temperatures, boundary grains or domain walls separate several ordered regions. To determine the transition from the ordered to the glassy state, the mean DL criterion was introduced to separate the ordered regions in the glassy state. We observed that at low temperatures, DL explodes, which is signature of the onset of a glassy state. Of course, this explosion can be observed only in a quenched Monte Carlo simulation. For the annealed Monte Carlo by decreasing the temperature, the system remains in an ordered state at low temperatures, and there is not enough energy to escape this situation. Our findings revealed that there are no considerable differences in the low-temperature behavior of the quenched and annealed Monte Carlo at $J/J' < 2$, Moreover, in strained and defective phosphorene structures, the locations of phase transitions shift with the strain strength. A finite-size scaling study is also provided to strengthen the validity of our results for an infinite lattice. Since every problem studied by the means of a 2D Ising model with competing interactions is analogous to planar π-ring systems, the observation of the spin configuration of phosphorene via the Ising model may contribute to the understanding of materials for AQC, qubits, and quantum computing.

Data availability

The datasets generated during and/or analyzed during the current study are available from the corresponding author on reasonable request.

Received: 21 May 2025; Accepted: 23 September 2025
Published online: 29 October 2025

References

1. Novoselov, K. S. et al. Electric field effect in atomically thin carbon films. *Science* **306**(5696), 666–669 (2004).
2. Acun, A. et al. Germanene: The germanium analogue of graphene. *J. Phys.: Condens. Matter* **27**(44), 443002 (2015).
3. Zhang, L. et al. Structural and electronic properties of germanene on MoS_2. *Phys. Rev. Lett.* **116**(25), 256804 (2016).
4. Ni, Z. et al. Tunable bandgap in silicene and germanene. *Nano Lett.* **12**(1), 113–118 (2012).
5. Kara, A. et al. A review on silicene—New candidate for electronics. *Surf. Sci. Rep.* **67**(1), 1–18 (2012).
6. Zhao, J. et al. Rise of silicene: A competitive 2D material. *Prog. Mater. Sci.* **83**, 24–151 (2016).
7. Oughaddou, H. et al. Silicene, a promising new 2D material. *Prog. Surf. Sci.* **90**(1), 46–83 (2015).
8. Chhowalla, M., Liu, Z. & Zhang, H. Two-dimensional transition metal dichalcogenide (TMD) nanosheets. *Chem. Soc. Rev.* **44**(9), 2584–2586 (2015).
9. Kou, L., Chen, C. & Smith, S. C. Phosphorene: Fabrication, properties, and applications. *J. Phys. Chem. Lett.* **6**(14), 2794–2805 (2015).
10. Carvalho, A. et al. Phosphorene: from theory to applications. *Nat. Rev. Materials* **1**(11), 1–16 (2016).
11. Das, S. et al. Tunable transport gap in phosphorene. *Nano Lett.* **14**(10), 5733–5739 (2014).
12. Liu, H. et al. Phosphorene: an unexplored 2D semiconductor with a high hole mobility. *ACS Nano* **8**(4), 4033–4041 (2014).
13. Bridgman, P. Two new modifications of phosphorus. *J. Am. Chem. Soc.* **36**(7), 1344–1363 (1914).
14. Keyes, R. W. The electrical properties of black phosphorus. *Phys. Rev.* **92**(3), 580 (1953).
15. Castellanos-Gomez, A. Black phosphorus: Narrow gap, wide applications. *J. Phys. Chem. Lett.* **6**(21), 4280–4291 (2015).
16. Tran, V., Soklaski, R., Liang, Y. & Yang, L. Layer-controlled band gap and anisotropic excitons in few-layer black phosphorus. *Phys. Rev. B* **89**(23), 235319 (2014).
17. Li, L. et al. Black phosphorus field-effect transistors. *Nat. Nanotechnol.* **9**(5), 372–377 (2014).
18. Fukuoka, S., Taen, T. & Osada, T. Electronic structure and the properties of phosphorene and few-layer black phosphorus. *J. Phys. Soc. Jpn.* **84**(12), 121004 (2015).
19. Guo, Z. et al. From black phosphorus to phosphorene: Basic solvent exfoliation, evolution of Raman scattering, and applications to ultrafast photonics. *Adv. Funct. Mater.* **25**(45), 6996–7002 (2015).
20. Qin, G. et al. Hinge-like structure induced unusual properties of black phosphorus and new strategies to improve the thermoelectric performance. *Sci. Rep.* **4**(1), 6946 (2014).
21. Yang, G., Li, L., Lee, W. B. & Ng, M. C. Structure of graphene and its disorders: A review. *Sci. Technol. Adv. Mater.* **19**(1), 613–648 (2018).
22. Jose, D. & Datta, A. Structures and chemical properties of silicene: unlike graphene. *Acc. Chem. Res.* **47**(2), 593–602 (2014).
23. Rodin, A., Carvalho, A. & Castro Neto, A. Strain-induced gap modification in black phosphorus. *Phys. Rev. Lett.* **112**(17), 176801 (2014).
24. Ramasubramaniam, A. & Muniz, A. R. Ab initio studies of thermodynamic and electronic properties of phosphorene nanoribbons. *Phys. Rev. B* **90**(8), 085424 (2014).
25. Kou, L., Ma, Y., Smith, S. C. & Chen, C. Anisotropic ripple deformation in phosphorene. *J. Phys. Chem. Lett.* **6**(9), 1509–1513 (2015).
26. Peralta, M., Freire, D. A., González-Hernández, R. & Mireles, F. Spin-orbit coupling effects in single-layer phosphorene. *Phys. Rev. B* **110**(8), 085404 (2024).
27. Kusmartsev, F. Destruction of the Meissner effect in granular high-temperature superconductors. *Phys. Rev. Lett.* **69**(15), 2268 (1992).
28. Farhi, E., Goldstone, J., Gutmann, S. & Sipser, M. Quantum computation by adiabatic evolution. arXiv preprint quant-ph/0001106 (2000).
29. Sahdane, T. et al. Magnetic phase transitions of phosphorene-like nano-structure: Monte Carlo study. *Philos. Mag.* **101**(16), 1836–1848 (2021).
30. Vahedi, J. & Peters, R. Edge magnetic properties of black phosphorene nanoribbons. *Phys. Rev. B* **103**(7), 075108 (2021).
31. Chaudhary, V., Neugebauer, P., Mounkachi, O., Lahbabi, S. & El Fatimy, A. Phosphorene—An emerging two-dimensional material: Recent advances in synthesis, functionalization, and applications. *Materials* **9**(3), 032001 (2022).
32. Margulis, V. A., Muryumin, E. & Gaiduk, E. Optical reflection, transmission and absorption properties of single-layer black phosphorus from a model calculation. *J. Opt.* **18**(5), 055102 (2016).
33. Popović, Z. S., Kurdestany, J. M. & Satpathy, S. Electronic structure and anisotropic Rashba spin-orbit coupling in monolayer black phosphorus. *Phys. Rev. B* **92**(3), 035135 (2015).
34. Fei, R. & Yang, L. Strain-engineering the anisotropic electrical conductance of few-layer black phosphorus. *Nano Lett.* **14**(5), 2884–2889 (2014).
35. Jiang, J.-W. & Park, H. S. Negative Poisson's ratio in single-layer black phosphorus. *Nat. Commun.* **5**(1), 4727 (2014).
36. Peng, X., Wei, Q. & Copple, A. Strain-engineered direct-indirect band gap transition and its mechanism in two-dimensional phosphorene. *Phys. Rev. B* **90**(8), 085402 (2014).
37. Qiao, J., Kong, X., Hu, Z.-X., Yang, F. & Ji, W. High-mobility transport anisotropy and linear dichroism in few-layer black phosphorus. *Nat. Commun.* **5**(1), 4475 (2014).
38. Lu, J. et al. Order–disorder transition in a two-dimensional boron–carbon–nitride alloy. *Nat. Commun.* **4**(1), 2681 (2013).
39. Wyatt, B. et al. Order to disorder transition due to entropy in layered and 2D carbides (2025).
40. Onsager, L. Crystal statistics. I. A two-dimensional model with an order-disorder transition. *Phys. Rev.* **65**(3–4), 117 (1944).
41. O'Hare, A., Kusmartsev, F. & Kugel, K. Two-dimensional Ising model with competing interactions: Phase diagram and low-temperature remanent disorder. *Phys. Rev. B Condens. Matter Mater. Phys.* **79**(1), 014439 (2009).
42. Wu, M., Yao, D.-X. & Wu, H.-Q. Exact diagonalization study of the anisotropic Heisenberg model related to $YbMgGaO_4$. *Phys. Rev. B* **103**(20), 205122 (2021).
43. Branco, N. & de Sousa, J. R. Real-space renormalization group study of the anisotropic antiferromagnetic Heisenberg model on a square lattice. *Phys. Rev. B* **62**(9), 5742 (2000).
44. Andreev, A. & Lifshits, I. Quantum theory of defects in crystals. *Zhur Eksper Teoret Fiziki* **56**(6), 2057–2068 (1969).
45. Van der Ploeg, S. et al. Controllable coupling of superconducting flux qubits. *Phys. Rev. Lett.* **98**(5), 057004 (2007).
46. Lucas, A. Ising formulations of many NP problems. *Front. Phys.* **2**, 5 (2014).
47. Heim, B., Rønnow, T. F., Isakov, S. V. & Troyer, M. Quantum versus classical annealing of Ising spin glasses. *Science* **348**(6231), 215–217 (2015).
48. Van der Ploeg, S. et al. Adiabatic quantum computation with flux qubits, first experimental results. *IEEE Trans. Appl. Supercond.* **17**(2), 113–119 (2007).
49. Ramazani, A., Shayeganfar, F., Kumar, A. & Fang, N. X. Terahertz Nonlinear Optics in Two-Dimensional Semi-hydrogenated SiB. arXiv preprint http://arxiv.org/abs/2109.00858 (2021).
50. Bishop, R. F., Farnell, D. J. & Parkinson, J. B. Phase transitions in the spin-half J_1–J_2 model. *Phys. Rev. B* **58**(10), 6394 (1998).

51. Roscilde, T., Feiguin, A., Chernyshev, A. L., Liu, S. & Haas, S. Anisotropy-induced ordering in the quantum J_1–J_2 antiferromagnet. *Phys. Rev. Lett.* **93**(1), 017203 (2004).
52. Schmalfuß, D., Darradi, R., Richter, J., Schulenburg, J. & Ihle, D. Quantum J_1–J_2 antiferromagnet on a stacked square lattice: Influence of the interlayer coupling on the ground-state magnetic ordering. *Phys. Rev. Lett.* **97**(15), 157201 (2006).
53. Viana, J. R. & de Sousa, J. R. Anisotropy effects in frustrated Heisenberg antiferromagnets on a square lattice. *Phys. Rev. B Condens. Matter Mater. Phys.* **75**(5), 052403 (2007).
54. Melzi, R. et al. $Li_2VO(Si,Ge)O_4$, a prototype of a two-dimensional frustrated quantum Heisenberg antiferromagnet. *Phys. Rev. Lett.* **85**(6), 1318 (2000).
55. Carretta, P. et al. Frustration-driven structural distortion in VOMoO 4. *Phys. Rev. B* **66**(9), 094420 (2002).
56. Kivelson, S. A. et al. How to detect fluctuating stripes in the high-temperature superconductors. *Rev. Mod. Phys.* **75**(4), 1201 (2003).
57. Tranquada, J. et al. Quantum magnetic excitations from stripes in copper oxide superconductors. *Nature* **429**(6991), 534–538 (2004).
58. Lilly, M., Cooper, K., Eisenstein, J., Pfeiffer, L. & West, K. Evidence for an anisotropic state of two-dimensional electrons in high Landau levels. *Phys. Rev. Lett.* **82**(2), 394 (1999).
59. Robertson, J. A., Kivelson, S. A., Fradkin, E., Fang, A. C. & Kapitulnik, A. Distinguishing patterns of charge order: Stripes or checkerboards. *Phys. Rev. B Condens. Matter Mater. Phys.* **74**(13), 134507 (2006).
60. Gao, S. et al. Atomic-scale strain manipulation of a charge density wave. *Proc. Natl. Acad. Sci.* **115**(27), 6986–6990 (2018).
61. Gye, G., Oh, E. & Yeom, H. W. Topological landscape of competing charge density waves in 2H-$NbSe_2$. *Phys. Rev. Lett.* **122**(1), 016403 (2019).
62. Zhu, J.-X. et al. Band narrowing and Mott localization in iron oxychalcogenides $La_2O_2Fe_2O(Se,S)_2$. *Phys. Rev. Lett.* **104**(21), 216405 (2010).
63. Nadiger, S., Jose, S. M., Ghosh, R., Kaur, I. & Nath, R. Stripe and checkerboard patterns in a stack of driven quasi-one-dimensional dipolar condensates. *Phys. Rev. A* **109**(3), 033309 (2024).
64. Dagotto, E. Complexity in strongly correlated electronic systems. *Science* **309**(5732), 257–262 (2005).
65. Comin, R. & Damascelli, A. Resonant x-ray scattering studies of charge order in cuprates. *Annu. Rev. Condens. Matter Phys.* **7**(1), 369–405 (2016).
66. Julien, M.-H. Magnetic fields make waves in cuprates. *Science* **350**(6263), 914–915 (2015).
67. Parker, C. V. et al. Fluctuating stripes at the onset of the pseudogap in the high-T_c superconductor $Bi_2Sr_2CaCu_2O_{8+x}$. *Nature* **468**(7324), 677–680 (2010).
68. Gerber, S. et al. Three-dimensional charge density wave order in $YBa_2Cu_3O_{6.67}$ at high magnetic fields. *Science* **350**(6263), 949–952 (2015).
69. Zheng, B.-X. et al. Stripe order in the underdoped region of the two-dimensional Hubbard model. *Science* **358**(6367), 1155–1160 (2017).
70. Dronova, M. G. et al. Three-dimensional checkerboard spin structure on a breathing pyrochlore lattice. *Phys. Rev. B* **109**(6), 064421 (2024).
71. Mézard, M., Parisi, G. & Virasoro, M. A. *Spin glass theory and beyond: An Introduction to the Replica Method and Its Applications* (World Scientific Publishing Company, 1987).
72. Binder, K. Applications of Monte Carlo methods to statistical physics. *Rep. Prog. Phys.* **60**(5), 487 (1997).
73. Newman, M. E. & Barkema, G. T. *Monte Carlo methods in statistical physics* (Clarendon Press, 1999).

Author contributions

F.S. and A.R. designed the theoretical aspects of this work and I.G. performed computational models; I.G., F.S., S.M.T. and A.R. analyzed the data and wrote the manuscript.

Declarations

Competing interests

The authors declare no competing interests.

Additional information

Supplementary Information The online version contains supplementary material available at https://doi.org/10.1038/s41598-025-21704-0.

Correspondence and requests for materials should be addressed to F.S.

Reprints and permissions information is available at www.nature.com/reprints.

Publisher's note Springer Nature remains neutral with regard to jurisdictional claims in published maps and institutional affiliations.